

Curvature Correlators in Nonperturbative 2D Lorentzian Quantum Gravity

J. van der Duin[†] and *R. Loll*^{†,*}

[†] Institute for Mathematics, Astrophysics and Particle Physics, Radboud University
Heyendaalseweg 135, 6525 AJ Nijmegen, The Netherlands.

and

^{*} Perimeter Institute for Theoretical Physics,
31 Caroline St N, Waterloo, Ontario N2L 2Y5, Canada.

Abstract

Correlation functions are ubiquitous tools in quantum field theory from both a fundamental and a practical point of view. However, up to now their use in theories of quantum gravity beyond perturbative and asymptotically flat regimes has been limited, due to difficulties associated with diffeomorphism invariance and the dynamical nature of geometry. We present an analysis of a manifestly diffeomorphism-invariant, nonperturbative two-point curvature correlator in two-dimensional Lorentzian quantum gravity. It is based on the recently introduced quantum Ricci curvature and uses a lattice regularization of the full path integral in terms of causal dynamical triangulations. We discuss some of the subtleties and ambiguities in defining connected correlators in theories of dynamical geometry, and provide strong evidence from Monte Carlo simulations that the connected two-point curvature correlator in 2D Lorentzian quantum gravity vanishes. This work paves the way for an analogous investigation in higher dimensions.

1 Introduction

With tools at our disposal to evaluate the gravitational path integral fully nonperturbatively in four dimensions, we can take an approach to quantum gravity that focuses on concrete physical questions rather than formal structural issues. The tried and tested method we have in mind here is lattice gravity based on causal dynamical triangulations (CDT), where the path integral is obtained as the scaling limit of a regularized sum over geometries [1–3]. CDT successfully navigates the subtleties of applying nonperturbative lattice methods to quantum gravity, including Wick rotation, conformal divergence and diffeomorphism invariance, and relies only on standard concepts and principles of quantum field theory. An invaluable part of CDT’s tool box are powerful Markov chain Monte Carlo methods, which can be and have been used extensively to compute gauge-invariant¹ observables in a near-Planckian regime.

Our best bet for relating quantum gravity at the Planck scale to the real world is arguably in early-universe cosmology. Here, CDT lattice gravity offers a promising perspective since it has produced strong evidence that the dimensionality [4–6], overall shape [7–9] and average curvature [10] of the quantum geometry emerging from the path integral are all compatible with those of a classical de Sitter universe. The presence of such quasi-classical behaviour (in the sense of expectation values) is quite remarkable, because the path integral is nonperturbative and manifestly background-independent, and local quantum fluctuations of geometry are large in the regime that is accessible to simulations.

An intrinsic difficulty in relating the nonperturbative quantum theory to cosmological considerations are the different scales involved and the distinct theoretical set-ups, including their associated observables. The early universe is usually described in terms of a smooth, de Sitter-like background metric with perturbative quantum fluctuations. Diffeomorphism-invariant observables can be constructed in a variety of ways, using gauge-fixing, gravitational dressing and relational constructions (see e.g. [11, 12] and references therein). Gauge-invariant observables exist also in a nonperturbative regime, but must be constructed differently due to the lack of a smooth manifold structure and the presence of large quantum fluctuations. The nature of the quantum geometry observed in CDT so far, for universes with a linear diameter $\lesssim 20 \ell_{\text{Pl}}$, suggests that at these scales a local tensorial description like in general relativity is neither adequate nor feasible *in principle*.

The most straightforward observables on the ensemble of nonsmooth metric spaces of the CDT path integral – nowhere differentiable spaces obtained in the continuum limit of piecewise flat triangulations – are given by spacetime averages of (quasi-)local properties. Concrete examples are the above-mentioned observ-

¹We will use the notions of diffeomorphism invariance and gauge invariance interchangeably.

ables whose expectation values match a classical limit, namely averages of the local Hausdorff and spectral dimensions, the volume and the so-called quantum Ricci curvature [13, 14].

Apart from providing valuable evidence for the existence of a classical limit, these observables also capture genuine quantum signatures, as is illustrated by the spectral dimension, whose expectation value at short distances exhibits a characteristic “dynamical dimensional reduction” away from its classical, large-scale value of 4 to a value compatible with 2 near the Planck scale [15]. This purely nonperturbative phenomenon, discovered in CDT, has since been corroborated qualitatively in other formulations and conjectured to be a universal property of quantum gravity [16]. However, there are at this stage no compelling ideas on how to relate this result to phenomenology at lower energies.

Let us emphasize that the availability of observables in nonperturbative quantum gravity *and* the ability to make quantitative statements about them amounts to significant progress in a field long characterized by an absence of computational tools beyond perturbation theory and by a reliance on abstract principles and preconceptions on what a fundamental theory of quantum gravity should (or should not) look like [17–20]. To strengthen this line of exploration further we would like to construct additional observables, which (i) are within the computational reach of current lattice methods, (ii) provide a more fine-grained understanding of quantum geometry, beyond global averages, and (iii) allow for a more direct connection with quantities relevant in the description of the early universe.

The subject of this paper is an observable that meets these requirements, namely a *diffeomorphism-invariant curvature correlator*. More precisely, we will investigate a prototype in two spacetime dimensions of the connected two-point correlator of the quantum Ricci scalar curvature in the nonperturbative gravitational path integral defined in terms of CDT. Its novelty is two-fold: correlation functions of nontrivial geometric observables have not been studied previously in a Lorentzian, causal lattice formulation, and until recently no well-defined notion of curvature was available in this context. The problem with the standard deficit-angle curvature inherited from Regge calculus is its divergent character in four-dimensional (C)DT (see [21] and references therein). By contrast, the quantum Ricci curvature, first introduced in [13], has been shown to be applicable in a nonsmooth, Planckian regime in four dimensions [10], while on smooth manifolds it allows one to recover the standard Ricci curvature [14].²

The aim of the present work is to implement and measure the correlator of the new quantum Ricci curvature for the first time, as a nontrivial test case and a stepping stone toward the physically relevant case in four dimensions. As we will see below, even in two dimensions the construction and analysis of

²The quantum Ricci curvature is designed for positive definite metric spaces, including the piecewise flat simplicial spaces of the CDT path integral obtained after the Wick rotation.

this observable presents interesting conceptual issues and technical challenges, providing a benchmark for what will be required in higher dimensions.

The remainder of this paper is organized as follows. In Sec. 2 we discuss some generalities on correlation functions in quantum gravity, with reference to previous, related work in nonperturbative lattice formulations. Sec. 3 recalls the main ingredients of formulating 2D Lorentzian quantum gravity as the continuum limit of a lattice regularization in terms of CDT, including the elementary building blocks, gluing rules, regularized path integral, Wick rotation, Monte Carlo moves and how to compute observables. In Sec. 4 we summarize important properties and applications of the quantum Ricci curvature, both in the continuum and on the lattice. In Sec. 5 we construct geometric two-point correlators and present our Monte Carlo measurements of curvature correlators in 2D CDT quantum gravity. We discuss different choices for their normalization and the subtraction procedure to obtain corresponding connected correlators, which are present due to the dynamical nature of geometry. We conclude in Sec. 6 with a summary and outlook. Two appendices contain technical details on how to determine the onset of finite-size effects and how to uniformly sample point pairs when measuring two-point correlators.

2 Correlation functions in quantum gravity

The physical content of a relativistic quantum field theory is captured entirely by the set of its *n-point correlation functions* or *correlators*, the vacuum expectation values of *n*-fold products of its local field operators. This is not only true for quantum fields on Minkowski spacetime, but also in a Wick-rotated formulation on flat Euclidean \mathbb{R}^4 , which is related to its Lorentzian counterpart by the Osterwalder-Schrader reconstruction theorem [22]. Also in the context of gravitational theories, *n*-point functions play an important role. Examples are correlators in perturbative quantum gravity [23, 24] and correlation functions of quantum fields on a cosmological background [12, 25].

What may be less well known is that correlation functions can also be defined in nonperturbative quantum gravity, in a manifestly background-independent and diffeomorphism-invariant way [26, 27]. Consider the case $n=2$, which we will focus on in this work. Given a local geometric scalar quantity $\mathcal{O}[g]$, say, a curvature scalar depending on the metric $g_{\mu\nu}$, the formal continuum expression for the (unnormalized) diffeomorphism-invariant two-point correlator of \mathcal{O} is given by

$$\langle G[\mathcal{O}, \mathcal{O}](r) \rangle = \int \mathcal{D}[g] e^{iS[g]} \int_M d^4x \sqrt{|g(x)|} \int_M d^4y \sqrt{|g(y)|} \mathcal{O}(x) \mathcal{O}(y) \delta(d_g(x, y) - r), \quad (1)$$

where the functional integration is over the space of all geometries $[g]$ (metrics g modulo diffeomorphisms on the given manifold M), with weights depending on the gravitational action $S[g]$, and $|g(x)|$ denotes the absolute value of the determinant of the metric g at the point x . Diffeomorphism invariance requires that the distance r appearing inside the Dirac δ -function is given in terms of the invariant geodesic distance d_g associated with the geometry g , and that the points x and y are integrated over spacetime, subject to the constraint of being a distance r apart. The viability of such diffeomorphism-invariant two-point functions, as well as an analogous version for matter correlators on fluctuating geometries, has been demonstrated in models of pure and matter-coupled Euclidean quantum gravity in two dimensions, formulated in terms of Dynamical Triangulations (DT) [28–33].

Geometric two-point functions have also been investigated in four dimensions, again in the context of Euclidean quantum gravity based on DT, with inconclusive results [34, 35] (see also [36]). Apart from the fact that it is unclear how to relate the underlying Euclidean to the physical, Lorentzian path integral, these pioneering studies suffer from at least two serious shortcomings, the absence to date of second-order phase transitions in 4D Euclidean quantum gravity, a necessary prerequisite for the existence of a continuum theory, and the absence of a well-defined notion of local curvature, to investigate invariant curvature-curvature correlators. The scalar curvature operator \mathcal{O} used in previous studies of 4D Euclidean quantum gravity was based on the deficit-angle prescription for curvature due to Regge [37]. However, as already mentioned in Sec. 1, this notion of curvature is not well-defined in the nonperturbative quantum theory, because it diverges in an uncontrolled manner in the infinite-volume limit [21, 38]. It is therefore unphysical and not suited for computing curvature correlators.

In this work, we exploit the progress that has been made since these early investigations. On the one hand, we will use the Lorentzian path integral as a starting point, whose lattice formulation in terms of CDT in four dimensions possesses several second-order phase transition lines [39–41]. On the other hand, we will use the novel quantum Ricci curvature, which has been shown to have an improved short-distance (UV) behaviour [10]. However, it is significantly more involved computationally, which means that its implementation requires particular attention.

3 Theoretical and computational set-up

The setting for our investigation of curvature correlators is the two-dimensional Lorentzian gravitational path integral, regularized in terms of CDT, which was first defined and solved analytically in [42]. It serves as a dimensionally reduced

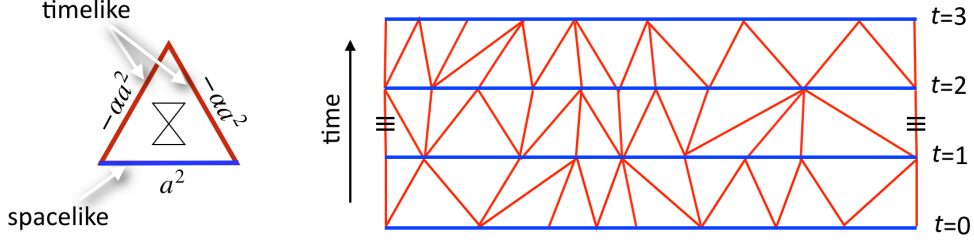


Figure 1: Minkowskian building block of 2D CDT, including a lightcone (left), and a piece of a CDT spacetime, consisting of a sequence of three triangulated strips, labelled by discrete proper time t (right). Left and right boundary should be identified as indicated, leading to a cylindrical topology $I \times S^1$.

and simplified toy model of full quantum gravity. We will summarize its essential properties below, and refer to [1, 43] for further technical details. Recall that classical gravity in two dimensions is trivial in the sense that for fixed topology – which we will assume – the Einstein-Hilbert action reduces to a volume term proportional to a cosmological constant Λ , and there are no nontrivial equations of motion or classical solutions. Nevertheless, the associated path integral

$$Z = \int \mathcal{D}[g] e^{iS[g]}, \quad S = -\Lambda \int_M d^2x \sqrt{|g|} \quad (2)$$

gives rise to a nontrivial model of quantum geometry, which is an excellent testing ground for new gauge-invariant observables. Its nonperturbative evaluation beautifully illustrates the power of random-geometric methods, where identical building blocks are assembled into piecewise flat manifolds in all possible ways, subject to certain gluing rules. They represent a regularized version of the configuration space of all geometries. In 2D CDT, the elementary building block is a flat Minkowskian isosceles triangle, with one spacelike and two timelike edges of squared edge length $\ell_s^2 = a^2$ and $\ell_t^2 = -\alpha a^2$ respectively, where a is the lattice spacing or UV cut-off and $\alpha > 0$ a positive constant (Fig. 1, left). These triangles (“two-simplices”) are glued together pairwise along edges of matching length, such that the resulting triangulated geometry T is a simplicial manifold with a well-defined causal structure, amounting to a discrete version of global hyperbolicity. For compact spatial S^1 -topology this is achieved by constructing each $(1+1)$ -dimensional geometry as a sequence of annular strips, labelled by a discrete “proper time” parameter t (Fig. 1, right).

In terms of these ingredients, the formal path integral (2) takes the explicit form

$$Z_{\text{CDT}}(\lambda) = \sum_T \frac{1}{C(T)} e^{-S_{\text{CDT}}(T)}, \quad S_{\text{CDT}}(T) = \lambda N_2(T), \quad (3)$$

where we have used the Wick rotation of CDT (analytic continuation $\alpha \mapsto -\alpha$ in the lower-half complex plane [1, 43]) to obtain a real partition function Z_{CDT} , which is easier to work with computationally and will be the setting for the work presented here. In the Euclideanized path integral (3), λ is the bare, dimensionless cosmological constant, multiplying the discrete volume of the triangulation T , given by the number $N_2(T)$ of triangles contained in it³, and $C(T)$ denotes the order of the automorphism group of T . The sum is over distinct Wick-rotated CDT geometries⁴ and can be performed in the continuum limit $a \rightarrow 0$ while tuning λ to its known critical value $\lambda_c = \ln 2$ from above according to

$$\lambda \rightarrow \lambda_c + a^2 \Lambda + O(a^3), \quad (4)$$

where Λ is the dimensionful renormalized cosmological constant [42]. Expectation values of geometric observables $\mathcal{O}(T)$ are computed according to

$$\langle \mathcal{O} \rangle = \frac{1}{Z_{\text{CDT}}} \sum_T \frac{1}{C(T)} \mathcal{O}(T) e^{-S_{\text{CDT}}(T)} \quad (5)$$

in the same limit. Sufficiently simple observables, like the spectral and Hausdorff dimension [42, 44] and the spectrum of the underlying quantum-mechanical Hamiltonian [1, 45] can be computed analytically, but this has not yet been possible for the quantum Ricci curvature. Following earlier work in 2D CDT on the average quantum Ricci curvature as a function of a local coarse-graining scale [46], the so-called curvature profile [47], we will investigate here its two-point correlator by a numerical analysis.

For computational convenience, we will adopt several standard choices. We will cyclically identify the time direction, such that the topology of the geometries is that of a two-torus $T^2 \equiv S^1 \times S^1$ (Fig. 2). Each one-dimensional spatial universe at constant integer time $t \in [0, 1, 2, \dots, t_{\text{tot}}]$, where times 0 and t_{tot} are identified, consists of a closed chain of $\ell(t) \geq 3$ spacelike edges. The simulations will be performed at various fixed two-volumes $N_2 \in [50\text{k}, 300\text{k}]$ and fixed numbers of time steps in such a way that the quotient $t_{\text{tot}}^2/N_2 \approx 0.16$ is approximately constant⁵, leading to an average spatial volume $\bar{\ell} = N_2/(2t_{\text{tot}})$ in the range $\bar{\ell} \in [280, 685]$.

Expectation values of geometric observables at fixed volume N_2 are given by

$$\langle \mathcal{O} \rangle_{N_2} = \frac{1}{Z_{N_2}} \sum_{T|N_2} \frac{1}{C(T)} \mathcal{O}(T), \quad Z_{N_2} = \sum_{T|N_2} \frac{1}{C(T)}, \quad (6)$$

³In general, $N_k(T)$ denotes the number of k -simplices in T .

⁴Note that these triangulations are piecewise flat manifolds of Riemannian signature after the analytic continuation, but still carry a memory of the original causal gluing rules.

⁵More precisely, the combinations used are $(N_2, t_{\text{tot}}) = (50\text{k}, 89), (100\text{k}, 126), (150\text{k}, 155), (200\text{k}, 179), (250\text{k}, 200)$ and $(300\text{k}, 219)$.

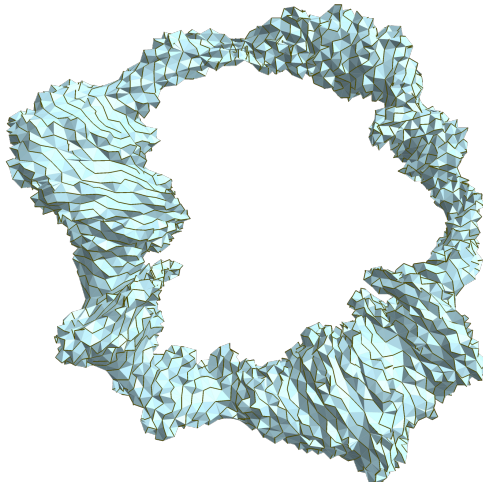


Figure 2: Typical 2D toroidal CDT configuration at $N_2 = 10k$, with spatial S^1 -slices of fluctuating length (marked by dark lines) and time extension $t_{\text{tot}} = 123$. Time is cyclically identified.

where the sums are over CDT configurations of volume N_2 , and the fixed-volume path integral Z_{N_2} is related to the CDT path integral (3) for cosmological constant λ by a Laplace transform,

$$Z_{\text{CDT}}(\lambda) = \sum_{N_2} e^{-\lambda N_2} Z_{N_2}. \quad (7)$$

The behaviour of observables in the limit of infinite volume is extrapolated from sequences of measurements for finite, increasing N_2 by using finite-size scaling, a standard tool for analyzing statistical systems (see e.g. [48]). We use a Monte Carlo Markov chain (MCMC) algorithm to generate sequences of independent CDT configurations, which allows us to approximate the expectation values (5) of observables by importance sampling from the CDT ensemble.

One hallmark of gravitational path integrals formulated in terms of (causal) dynamical triangulations is the fact that no coordinates are needed to describe the triangulated manifolds. The geometry of the individual building blocks is uniquely fixed by their geodesic edge lengths, and is complemented by connectivity data which specify the neighbourhood relations between pairs of building blocks. An important consequence in the present context is the absence of any nontrivial diffeomorphism- or coordinate-symmetry that needs to be taken into account when evaluating the path integral. This leads to an important simplification compared to the situation in continuum path integrals, where such a gauge redundancy cannot be avoided. Note that during numerical simulations it becomes necessary to attach labels to the (sub-)simplices of a triangulation, which

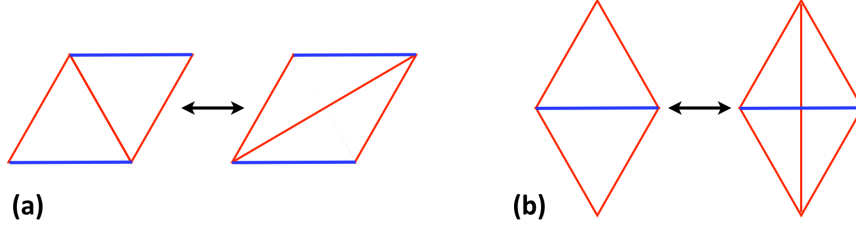


Figure 3: The two standard Monte Carlo moves in 2D CDT, the flip move (a) and the 2-4 or 4-2 move (b), depending on the direction of the arrow.

might be seen as analogous to using coordinates. However, these unphysical labels are discrete and the ensuing redundancy can be taken care of in a straightforward way in the computer algorithm by working with labelled triangulations and appropriately taking relabelling multiplicities into account [1, 49].

The computer code used in this work was written from scratch in the Rust programming language [50]. Source code and accompanying documentation are available via a GitLab repository [51]. It was tested thoroughly by measuring several standard quantities (vertex degree distribution of a CDT lattice, Hausdorff and spectral dimensions), and comparing them to the analytically known values⁶ as well as previous measurements, yielding compatible results.⁷

We will not describe all details of the Monte Carlo simulation, which do not deviate significantly from earlier implementations, and point the interested reader to reference [53]. The only novelty we introduced in the 2D simulations is a set of ergodic, *volume-preserving* Monte Carlo moves, thereby avoiding the need to perform simulations in a small window $[N_2 - \Delta N_2, N_2 + \Delta N_2]$ around a target volume N_2 . Recall that the standard moves to create a Markov chain $\{T_0, T_1, T_2, \dots\}$ of CDT configurations are two types of local alterations of a triangulation, the flip move (Fig. 3a) and the 2-4 move together with its inverse 4-2 move (Fig. 3b) [43]. The latter is not volume-preserving, since it adds or removes two triangles. We have substituted it by a nonlocal move that combines the application of a 2-4 move with the simultaneous application of a 4-2 move in a non-overlapping location on the same triangulation T_i , and leaves N_2 invariant.⁸ It is easy to show that this new move together with the flip move is ergodic in the CDT ensemble of a given volume N_2 and number t_{tot} of spatial slices. A systematic discussion for 2D and 3D CDT of the Metropolis-Hastings algorithm, Monte Carlo

⁶In the infinite-volume limit, the probability distribution of the vertex degree (coordination number) c is given by $p[c] = \frac{c-3}{2^{c-2}}$ for $c \geq 4$ [52]. The Hausdorff dimension d_H and spectral dimension d_S are both equal to 2 [42, 44].

⁷We found a discrepancy between the measured and analytically known Hausdorff dimension, which was also the case in previous investigations, see [53] for further details.

⁸We thank T. Budd for suggesting this construction.

moves, detailed balance conditions, optimal data storage and retrieval, and issues of tuning, thermalization and measurement can be found in [54].

4 Quantum Ricci curvature

Given the central importance of curvature in general relativity, one may wonder whether there is a notion of *quantum curvature* that can play an analogous role in nonperturbative quantum gravity. In view of the second-order nature of the classical Riemann tensor, it is unclear a priori how to associate a local curvature with a nonsmooth space, like those occurring in the CDT path integral. To be useful from a physical point of view, such a notion should be well-defined and finite in a strongly quantum-fluctuating microscopic regime and at the same time relate to standard notions of curvature on macroscopic scales, where geometry is smooth and classical. The quantum Ricci curvature (QRC) introduced in [13] has been shown to satisfy both criteria. It is a quasi-local quantity which relies on distance and volume measurements, but does not require smoothness or the availability of tensor calculus. A comprehensive review of the QRC and its applications, and of other attempts to define curvature in nonperturbative (C)DT quantum gravity can be found in [21]; below we will give a compact summary of the properties of the QRC that are relevant to the construction of the curvature correlator.

The QRC is based on the geometric insight that in a Riemannian space, in the presence of positive (negative) Ricci curvature, the distance – appropriately defined – between two sufficiently close and sufficiently small geodesic spheres is smaller (bigger) than the distance between their centres [55]. This can be turned around to *define* a generalized notion of Ricci curvature on general, non-smooth metric spaces [56]. Exploiting this idea, the QRC uses as a distance the *average sphere distance* \bar{d} . For two $(D-1)$ -spheres S_p^δ and $S_{p'}^\delta$ of radius δ on a D -dimensional Riemannian manifold $(M, g_{\mu\nu})$, with centres p and p' , it is defined as [13]

$$\bar{d}(S_p^\delta, S_{p'}^\delta) := \frac{1}{\text{vol}(S_p^\delta)} \frac{1}{\text{vol}(S_{p'}^\delta)} \int_{S_p^\delta} d^{D-1}q \sqrt{h} \int_{S_{p'}^\delta} d^{D-1}q' \sqrt{h'} d_g(q, q'), \quad d_g(p, p') = \varepsilon, \quad (8)$$

which is simply the distance average of all point pairs $(q, q') \in S_p^\delta \times S_{p'}^\delta$. In relation (8), h and h' denote the determinants of the induced metrics on the two spheres, $\text{vol}(S^\delta)$ denotes the volume of the sphere with respect to the corresponding induced metric, and $d_g(q, q')$ is the geodesic distance of the points q and q' with respect to the metric g .

Our application will involve a simplicial implementation of (8) for $D=2$ and for the case $\varepsilon=0$, such that $p'=p$ and the two spheres coincide. The latter is a

convenient choice since we will only be interested in correlators of the direction-independent (quantum) Ricci scalar, and not the full quantum Ricci curvature, although for simplicity we will still refer to it as “QRC” in what follows. For vanishing ε , (8) measures the distance of the sphere S_p^δ to itself. To exhibit the relation of this quantity with the local Ricci scalar $R(p)$ in the continuum case, we divide the expression for \bar{d} by δ to obtain the *normalized average sphere distance*. Evaluating it at a point p of a 2D Riemannian manifold as a power series in δ yields

$$\bar{d}(S_p^\delta, S_p^\delta)/\delta = \frac{4}{\pi} - \frac{\delta^2}{9\pi}R(p) + O(\delta^3) \approx 1.273 - 0.0354\delta^2 R(p) + O(\delta^3), \quad (9)$$

as may be verified, say, by a computation in Riemann normal coordinates [57]. This expression is valid for δ sufficiently small such that the geodesics involved in the measurement of pairwise distances exist and are unique. The particular value of the constant term is related to our choice of sphere distance [13]. Apart from this finite rescaling of the constant term, the expansion (9) captures our earlier statement about the geometric insight underlying the QRC, since the coefficient of the lowest-order “correction” term proportional to δ^2 to the constant term is a negative number times the Ricci scalar. Higher-order terms in the δ -expansion (9) depend on the Ricci scalar and its covariant derivatives. In other words, for vanishing Ricci scalar the function \bar{d}/δ will be constant in δ , while for positive (negative) Ricci scalar it will initially decrease (increase) as a function of δ .

In terms of the normalized averaged sphere distance (9), the *quantum Ricci curvature* $K_q(p; \delta)$ is defined by

$$\bar{d}(S_p^\delta, S_p^\delta)/\delta =: c_q(1 - K_q(p; \delta)), \quad (10)$$

where $c_q := \lim_{\delta \rightarrow 0} \bar{d}/\delta$ in the smooth case and K_q captures the δ -dependent part of the left-hand side. The subscript “ q ” stands for “quantum”, although the context at this stage is not (yet) the quantum theory. On smooth manifolds, c_q is a constant satisfying $0 < c_q < 2$ which only depends on the dimension. However, the main motivation for the definition (10) is that it allows us to associate a curvature with more general metric spaces, and piecewise flat triangulated spaces in particular. On such a triangulation, distances and volumes come in discrete lattice units. On the 2D CDT configurations considered here, we will use the *geodesic link distance* $d(q, p)$ between pairs (q, p) of lattice vertices, which is given by the number of edges in the shortest path along edges between q and p .⁹ The geodesic sphere S_p^δ of radius δ with central vertex p is defined as the set of all vertices q that have link distance δ to p , and the discrete volume $N_0(S_p^\delta)$ of

⁹Note that without loss of generality the triangular building blocks after the Wick rotation can be taken to be equilateral, implying that all edges have length a .

S_p^δ is the number of vertices contained in it. In terms of these ingredients, the normalized average sphere distance for $\varepsilon=0$ becomes¹⁰

$$\bar{d}(S_p^\delta, S_p^\delta)/\delta = \frac{1}{N_0(S_p^\delta)^2} \sum_{q \in S_p^\delta} \sum_{q' \in S_p^\delta} d(q, q')/\delta. \quad (11)$$

As one would expect, this quantity suffers from lattice artefacts for small δ , i.e. a behaviour that is sensitive to the way the discretization has been set up. Investigations of the QRC on various classical and dynamically triangulated lattices in 2D have consistently found significant lattice artefacts in a region $\delta \lesssim 5$ [13, 14, 46]. Since we are interested in the continuum limit of these regularized models, we should discard data points from this region. We also need to define a suitable lattice analogue of the limit $\delta \rightarrow 0$ when extracting the QRC via relation (10), as well as take into account that the value of c_q is not universal, but depends on the discretization [13].

For nonclassical triangulations, which are not designed to approximate a specific classical manifold, we do not know the functional form in δ of the normalized average sphere distance $\bar{d}(S_p^\delta, S_p^\delta)/\delta$ a priori. In particular, there is no guarantee that in a δ -window outside the region of lattice artefacts it can be fitted to a curve of the form $\gamma(\delta) = \alpha - \beta\delta^2 + h.o.$, for constants α, β , as a function of the distance δ and in generic points p . If such a fit is possible, it constitutes nontrivial evidence for the presence of a positive, negative or vanishing curvature compatible with that of a continuum manifold, at least when the distance δ scales canonically, i.e. behaves like a length.¹¹ If such a fit is not possible, a positive or negative deviation of \bar{d}/δ from constancy according to our definition (10) still gives rise to a nonvanishing quantum Ricci curvature, characterizing the metric space in question, but its geometric (continuum) interpretation may be less clear-cut. This latter situation appears to be realized in 2D CDT [46], as we will discuss later in this section. This is not completely surprising, since 2D quantum gravity is a pure quantum theory; the Einstein-Hilbert action in 2D does not possess nontrivial geometric solutions, which means that there are no classical spacetimes that can be obtained from the quantum theory in some classical limit.

For use in the quantum theory, we must construct diffeomorphism-invariant observables from these ingredients. The most straightforward way of doing this is to take the average \bar{d}_{av} over the triangulation T of the average sphere distance. Its normalized version gives rise to what has been dubbed the *curvature profile*

¹⁰Since the local quantities we will consider are mainly associated with vertices of the triangulation, any averages will typically involve the number $N_0(T)$ of vertices. On a torus, this is related to the number $N_2(T)$ of triangles in T by $N_2(T) = 2N_0(T)$.

¹¹In quantum applications, this will also involve a finite-size scaling analysis and a substitution of dimensionless lattice quantities by their dimensionful counterparts.

of T [47],

$$\bar{d}_{\text{av}}(\delta)/\delta := \frac{1}{N_0(T)} \sum_{p \in T} \bar{d}(S_p^\delta, S_p^\delta)/\delta, \quad (12)$$

which can be used to extract an average QRC $K_{\text{av}}(\delta)$ via

$$\bar{d}_{\text{av}}(\delta)/\delta =: c_{\text{av}}(1 - K_{\text{av}}(\delta)), \quad (13)$$

where the constant c_{av} should be fixed appropriately, e.g. by the value of $\bar{d}_{\text{av}}/\delta$ just outside the region of lattice artefacts.

The expectation value of the curvature profile (13) has been investigated for Euclidean DT quantum gravity in 2D [14], and for Lorentzian CDT quantum gravity in 2D [46] and 4D [10]. In all cases the standard QRC, based on the direction-dependent average sphere distance (8) with $\varepsilon = \delta$ was used, followed by a directional averaging. We have repeated the measurements of [46] for 2D CDT, as a further cross-check of our code, and found excellent agreement, as long as δ is sufficiently small to not be affected by finite-size effects¹². The latter arise because of the compactness of the triangulations in both the time and spatial directions. When the spheres involved in the sphere distance measurements become sufficiently large, there will be point pairs (q, q') contributing to (11) whose associated geodesic – which we have defined as the *globally* shortest path between q and q' – will run around the “back side” of the torus, i.e. take a “topological shortcut” that would not be available if the torus was cut open to remove the compactification. For even larger δ , the spheres themselves will eventually start wrapping around the compact directions, giving rise to self-overlaps.

Since we are primarily interested in local curvature properties, we want to control and eliminate such global, finite-size effects as much as possible. This is not completely straightforward in the case at hand because the geometry fluctuates: although the average size $\bar{\ell}$ of spatial slices is determined by the two-volume N_2 and time extension t_{tot} , fluctuations $\Delta\ell(t)$ are large [42], which means that the length of the shortest closed geodesic winding once around the spatial direction depends on the configuration T and will typically be much smaller than $\bar{\ell}$. One could in principle keep track of the nature of the geodesic of each point pair (q, q') , but this is computationally costly. Instead, the strategy developed in [46] was to establish an upper bound δ_{max} on the sphere radii δ for given N_2 and t_{tot} , such that for $\delta \leq \delta_{\text{max}}$ occurrences of topological shortcuts are sufficiently rare to not distort measurements of the average sphere distance significantly.

In the present work, we have used a slight variant of the criterion in [46] to find a set $\{\delta_{\text{max}}\}$ of such thresholds, see [53] for details. For lattice volumes $N_2 \in [50\text{k}, 300\text{k}]$, they lie in the range $\delta_{\text{max}} \in [12, 35]$. In the plots of the expectation

¹²and taking into account that a different method of sampling pairs of spheres was used in [46], see Appendix B for further discussion

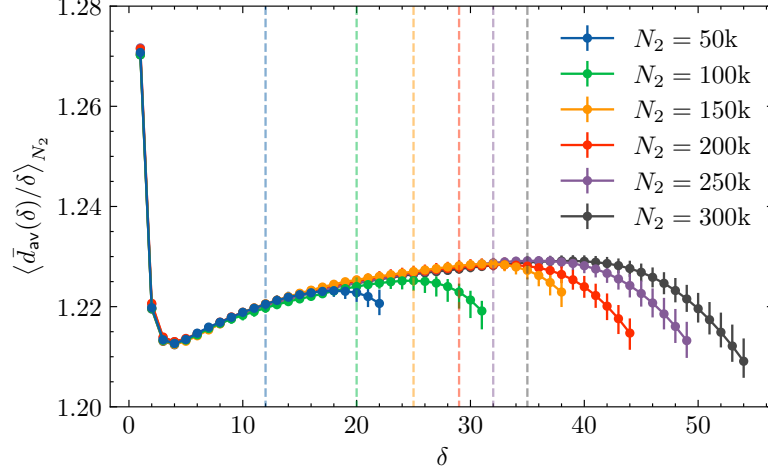


Figure 4: Curvature profile $\langle \bar{d}_{\text{av}}(\delta)/\delta \rangle_{N_2}$ for $\varepsilon=0$ measured in 2D CDT ensembles of fixed volume $N_2 \in [50\text{k}, 300\text{k}]$. The vertical dashed lines indicate thresholds δ_{max} for the sphere radii, below which finite-size effects are negligible for the corresponding volume N_2 . (Here and in subsequent figures, discrete data points are connected by straight line segments for easier visualization.)

value $\langle \bar{d}_{\text{av}}(\delta)/\delta \rangle_{N_2}$ of the curvature profile (or normalized average sphere distance) shown in Fig. 4 they are indicated by vertical dashed lines. The measurements of the curvature correlators presented in Sec. 5 below use only values for δ that lie well below these thresholds.

The curvature profile of Fig. 4 we have measured for $\varepsilon=0$ is qualitatively very similar to the standard case of the QRC with $\varepsilon=\delta$ investigated previously [46], and consistent with these earlier findings. The region $\delta \lesssim 5$ shows a rapid fall-off that is virtually identical for all volumes, a typical lattice artefact. Beyond it, each of the curves increases gently until eventually dropping off again, the latter being a known finite-size effect due to the underlying compactified spacetime topology. Within error bars, the curves coincide within their relevant N_2 -dependent ranges $\delta \in [5, \delta_{\text{max}}]$. The joint enveloping curve of the curvature profile increases, with a decreasing slope for growing δ , similar to what was observed in [46], and indicating the presence of negative curvature. However, in line with our remarks earlier in this section the function $\langle \bar{d}_{\text{av}}(\delta)/\delta \rangle_{N_2}$ beyond $\delta=5$ appears to be concave. It therefore cannot be fitted to a quadratic deviation from constancy of the form $-\beta\delta^2$, $\beta < 0$, which would indicate compatibility with a negative average (continuum) Ricci scalar, because this is associated with a convex curvature profile. We conclude that 2D CDT exhibits the presence of a nonvanishing, negative average QRC, as captured by relation (13).¹³ This motivates the study of curvature

¹³Note that this does not contradict the Gauss-Bonnet theorem, since there is no 2D classical

correlators based on the QRC, which we will turn to next.

5 Connected correlators

The definition and implementation of geometric, invariant two-point functions in quantum gravity comes with some subtleties and ambiguities, which we will discuss before presenting the outcomes of our measurements for the curvature correlators. They are related to the fact that geometry fluctuates and there is no a priori fixed background geometry. The resulting nonuniqueness of the correlation functions concerns their normalization, the role of manifold versus ensemble average and the subtraction prescription to obtain connected correlators. Different choices lead to inequivalent prescriptions of correlators at the level of the regularized theory. Whether or not they also lead to physically inequivalent results in the continuum limit has to be investigated in detail for a given observable and a given quantum gravity model. As we will see below, we found good evidence in the case at hand that the differences between these choices become negligible for large volumes N_2 and distances r , but this was by no means a foregone conclusion.

5.1 Classical preliminaries

We will temporarily revert to a continuum formulation in terms of a two-dimensional compact Riemannian manifold $(M, g_{\mu\nu})$ to introduce some key elements of the correlator construction. Given two local scalar functions $\mathcal{O}_1(x)$, $\mathcal{O}_2(x)$ of the metric $g_{\mu\nu}$, we can define the diffeomorphism-invariant quantity

$$G_g[\mathcal{O}_1, \mathcal{O}_2](r) := \int_M d^2x \sqrt{g(x)} \int_M d^2y \sqrt{g(y)} \mathcal{O}_1(x) \mathcal{O}_2(y) \delta(d_g(x, y) - r), \quad (14)$$

which may be thought of as a “classical two-point function” of \mathcal{O}_1 and \mathcal{O}_2 , depending on the geodesic distance r and the geometry g (metric modulo diffeomorphisms). The integrations over the locations of the two points x and y are necessary to obtain a diffeomorphism-invariant quantity, which is also required to make any subsequent ensemble average meaningful. We are not suggesting that (14) is an interesting observable from the point of view of classical general relativity, but only that it is a useful ingredient of the quantum theory, where we will consider expectation values of invariant observables in the (nonperturbative) vacuum state of the theory. By construction, $G_g[\mathcal{O}_1, \mathcal{O}_2](r)$ is symmetric in its

manifold or geometry associated with the continuum limit of 2D CDT. Alternative notions of (quantum) curvature in 2D, including Regge’s deficit-angle curvature [37] or variants of the QRC [58], may behave differently.

two functional arguments. Since the manifold is assumed to have a finite volume

$$V_g = \int_M d^2x \sqrt{g}, \quad (15)$$

(14) must vanish for sufficiently large r , whenever there are no more point pairs in M that are sufficiently far apart. Noting that the constant function $\mathcal{O}(x)=1$ is a special case, one can construct two classical correlators that will play an important role in what follows. For two insertions of the unit function one obtains

$$\begin{aligned} G_g[1, 1](r) &= \int_M d^2x \sqrt{g(x)} \int_M d^2y \sqrt{g(y)} \delta(d_g(x, y) - r) \\ &= \int_M d^2x \sqrt{g(x)} \text{vol}(S_x^r) = V_g \overline{\text{vol}(S^r)}|_g, \end{aligned} \quad (16)$$

which is a measure of the number of all point pairs with mutual distance r in the geometry g . The overbar in (16) denotes the diffeomorphism-invariant manifold average,

$$\overline{\mathcal{O}}|_g := \frac{1}{V_g} \int_M d^2x \sqrt{g(x)} \mathcal{O}(x), \quad (17)$$

where our notation highlights its g -dependence for added clarity. If one of the functions is the unit function, we have

$$\begin{aligned} G_g[\mathcal{O}, 1](r) &\equiv G_g[1, \mathcal{O}](r) = \int_M d^2x \sqrt{g(x)} \int_M d^2y \sqrt{g(y)} \mathcal{O}(x) \delta(d_g(x, y) - r) \\ &= \int_M d^2x \sqrt{g(x)} \mathcal{O}(x) \text{vol}(S_x^r), \end{aligned} \quad (18)$$

which, up to an overall factor of V_g , is the manifold average of the product of $\mathcal{O}(x)$ with a nonlocal weight factor equal to the size of the sphere S_x^r of radius r centred at x . The source of this nonlocality is the geodesic distance $d_g(x, y)$ between point pairs (x, y) , which depends nonlocally on the metric.

A “connected” version of the classical two-point function (14) is obtained by substituting the functional arguments $\mathcal{O}_i(x)$ by the deviations from their means $\overline{\mathcal{O}}_i|_g$, yielding

$$G_g^c[\mathcal{O}_1, \mathcal{O}_2](r) := \int_M d^2x \sqrt{g(x)} \int_M d^2y \sqrt{g(y)} (\mathcal{O}_1(x) - \overline{\mathcal{O}}_1|_g)(\mathcal{O}_2(y) - \overline{\mathcal{O}}_2|_g) \delta(d_g(x, y) - r), \quad (19)$$

which again is of the form of a diffeomorphism-invariant twofold manifold integral. In terms of the previous two-point functions (14), (16) and (18), this expression can be written as

$$\begin{aligned} G_g^c[\mathcal{O}_1, \mathcal{O}_2](r) &= \\ &G_g[\mathcal{O}_1, \mathcal{O}_2](r) - \overline{\mathcal{O}}_1|_g G_g[\mathcal{O}_2, 1](r) - \overline{\mathcal{O}}_2|_g G_g[\mathcal{O}_1, 1](r) + \overline{\mathcal{O}}_1|_g \overline{\mathcal{O}}_2|_g G_g[1, 1](r). \end{aligned} \quad (20)$$

Note in particular the nature of the “mixed” terms depending on $G_g[\mathcal{O}_i, 1](r)$, which depend nontrivially on the metric, as we have pointed out above. This dependence becomes trivial when the metric is constant, in the sense of being maximally symmetric, i.e. having a maximal number of Killing vectors. Specializing to the two-dimensional case at hand, maximal symmetry of the 2D geometry g on M implies that $\text{vol}(S_x^r)$ does not depend on x , and $G_g[\mathcal{O}_i, 1]$ factorizes according to

$$G_g[\mathcal{O}_i, 1](r) = \text{vol}(S^r)|_g \int_M d^2x \sqrt{g(x)} \mathcal{O}_i(x) = \text{vol}(S^r)|_g V_g \overline{\mathcal{O}}_i|_g \quad [g \text{ max. symmetric}], \quad (21)$$

where $\text{vol}(S^r)|_g = \overline{\text{vol}(S^r)}|_g$. As a consequence, the last three terms on the right-hand side of (20) are all equal (up to their signs) and the expression simplifies to

$$G_g^c[\mathcal{O}_1, \mathcal{O}_2](r) = G_g[\mathcal{O}_1, \mathcal{O}_2](r) - V_g \text{vol}(S^r)|_g \overline{\mathcal{O}}_1|_g \overline{\mathcal{O}}_2|_g \quad [g \text{ max. symmetric}]. \quad (22)$$

A further simplification occurs when one considers normalized versions of these classical expressions, which we will denote by \tilde{G}_g and \tilde{G}_g^c . A natural normalization for given r is obtained by dividing by expression (16),

$$\tilde{G}_g[\mathcal{O}_1, \mathcal{O}_2](r) := \frac{G_g[\mathcal{O}_1, \mathcal{O}_2](r)}{G_g[1, 1](r)}, \quad (23)$$

and similarly for \tilde{G}_g^c . For maximally symmetric $g_{\mu\nu}$ this yields the simple form

$$\tilde{G}_g^c[\mathcal{O}_1, \mathcal{O}_2](r) = \tilde{G}_g[\mathcal{O}_1, \mathcal{O}_2](r) - \overline{\mathcal{O}}_1|_g \overline{\mathcal{O}}_2|_g \quad [g \text{ max. symmetric}]. \quad (24)$$

5.2 Correlators in 2D CDT quantum gravity

After these preliminary classical considerations we now turn to the definition of genuine two-point correlation functions in the (fixed-volume) quantum ensemble of 2D CDT. We will largely adhere to the notation of the previous subsection, where r will now refer to the geodesic link distance, the delta function of r is replaced by a Kronecker delta, and the dependence on a geometry g is replaced by the dependence on a triangulated CDT configuration T . (Quasi-)local quantities \mathcal{O} will be associated with vertices $x \in T$, where we associate with each vertex a volume weight 1. As a consequence, (simplicial) manifold averages are given by

$$\overline{\mathcal{O}}|_T = \frac{1}{N_0(T)} \sum_{x \in T} \mathcal{O}(x), \quad (25)$$

and the lattice implementation of the classical two-point function (14) has the form

$$G_T[\mathcal{O}_1, \mathcal{O}_2](r) := \sum_{x, y \in T} \mathcal{O}_1(x) \mathcal{O}_2(y) \delta_{d(x, y), r}. \quad (26)$$

We will always compute expectation values of observables in the fixed-volume ensemble, as defined by (6). For simplicity of notation we will drop the subscript N_2 , i.e. henceforth $\langle \cdot \rangle_{N_2} \equiv \langle \cdot \rangle$. With this understanding, a natural definition of an (unnormalized) connected two-point correlator, inspired by (19) and (20), is

$$\begin{aligned} \langle G_T^c[\mathcal{O}_1, \mathcal{O}_2](r) \rangle &= \langle G_T[\mathcal{O}_1, \mathcal{O}_2](r) \rangle - \langle \overline{\mathcal{O}}_1|_T G_T[\mathcal{O}_2, 1](r) \rangle \\ &\quad - \langle \overline{\mathcal{O}}_2|_T G_T[\mathcal{O}_1, 1](r) \rangle + \langle \overline{\mathcal{O}}_1|_T \overline{\mathcal{O}}_2|_T G_T[1, 1](r) \rangle. \end{aligned} \quad (27)$$

Due to its quantum nature, the physical interpretation of this correlator is quite different from that of its classical precursor (19). If one has only worked with correlation functions of nongravitational quantum fields on a fixed Minkowskian or Euclidean background, an unexpected feature of (27) may be the presence of nontrivial correlations involving the unit operator, a quantity that does not depend on the dynamical field of the theory! The generic occurrence of such correlations was already noted in earlier treatments of Euclidean lattice gravity [33, 34]. However, a closer examination reveals that their origin is not the insertion of the unit operator at x or y , but the r -dependence of $G_T[\cdot, \cdot](r)$. The distance r refers to the length of the shortest geodesic between x and y and therefore depends on the metric in a nonlocal way. In other words, the so-called “two-point function” $\langle G_T[\mathcal{O}_1, \mathcal{O}_2](r) \rangle$ has a *threefold* dependence on geometry, through the local geometric operators \mathcal{O}_1 , \mathcal{O}_2 and through the nonlocal distance operator r that appears as an argument of the Kronecker delta. Quantum fluctuations of the geometry affect all of them, generally giving rise to nontrivial correlations. This is an intrinsic feature of correlators in quantum gravity, whether treated perturbatively or nonperturbatively, including correlators of quantum matter coupled to quantum gravity. In all cases, diffeomorphism invariance requires that correlators should not depend on a coordinate, but on a physical distance, which in turn implies a nontrivial and nonlocal dependence on the underlying quantized metric field. This is most transparent in an approach like ours, where the correlation functions depend explicitly on the geodesic distance, as opposed to, say, gauge-fixed formulations.¹⁴

Furthermore, the last three terms on the right-hand side of (27) also involve correlations between configuration averages $\overline{\mathcal{O}}_i|_T$ and either $G_T[\mathcal{O}_i, 1](r)$ or $G_T[1, 1](r)$. Since all of these quantities are already T -averaged individually, one would expect their correlations to be much smaller than those captured by the expectation values $\langle G_T[\cdot, \cdot](r) \rangle$. It turns out that eliminating these correlations, by substituting $\langle \overline{\mathcal{O}}_1|_T G_T[\mathcal{O}_2, 1](r) \rangle \longrightarrow \langle \overline{\mathcal{O}}_1|_T \rangle \langle G_T[\mathcal{O}_2, 1](r) \rangle$ etc., is equivalent to using a variant of the connected correlator (27), which is equally well motivated a priori. It is obtained by substituting the T -averaged mean values $\overline{\mathcal{O}}_i|_T$, whose

¹⁴For examples of continuum treatments of gravitational correlators depending on geodesic distances, see [59, 60] and references therein.

continuum version we subtracted in the classical formula (19), by their quantum (=ensemble) means $\langle \bar{\mathcal{O}}_i|_T \rangle$, resulting in

$$\begin{aligned} \langle G_{T,q}^c[\mathcal{O}_1, \mathcal{O}_2](r) \rangle &= \langle G_T[\mathcal{O}_1, \mathcal{O}_2](r) \rangle - \langle \bar{\mathcal{O}}_1|_T \rangle \langle G_T[\mathcal{O}_2, 1](r) \rangle \\ &\quad - \langle \bar{\mathcal{O}}_2|_T \rangle \langle G_T[\mathcal{O}_1, 1](r) \rangle + \langle \bar{\mathcal{O}}_1|_T \rangle \langle \bar{\mathcal{O}}_2|_T \rangle \langle G_T[1, 1](r) \rangle, \end{aligned} \quad (28)$$

where the subscript q stands for “quantum”. There is yet another variant that has been proposed in the literature [34,61], namely to use as a mean the ensemble-averaged r -dependent normalized, weighted averages

$$\langle \tilde{G}_T[\mathcal{O}_i, 1](r) \rangle := \left\langle \frac{G_T[\mathcal{O}_i, 1](r)}{G_T[1, 1](r)} \right\rangle = \left\langle \frac{\sum_{x,y \in T} \mathcal{O}_i(x) \delta_{d(x,y),r}}{\sum_{x,y \in T} \delta_{d(x,y),r}} \right\rangle, \quad (29)$$

which amounts to substituting all instances of $\langle \bar{\mathcal{O}}_i|_T \rangle$ in (28) by $\langle \tilde{G}_T[\mathcal{O}_i, 1](r) \rangle$. We will not consider this prescription further here, but we have verified that the normalized version of the resulting connected curvature correlator away from the regions with discretization and finite-size effects leads to results very similar to those for the normalized version of the correlator (28) [53].

Turning next to the normalization of the connected correlators, a natural normalization for a given geometry and distance r we have already used in (23) and (29) is a division by $G_g[1, 1](r)$ and $G_T[1, 1](r)$ respectively. It has two different quantum implementations, depending on whether we normalize before or after taking the ensemble average. If we normalize the correlator (27), this leads to the two options

$$\mathcal{G}[\mathcal{O}_1, \mathcal{O}_2, r] := \langle \tilde{G}_T^c[\mathcal{O}_1, \mathcal{O}_2](r) \rangle = \left\langle \frac{G_T^c[\mathcal{O}_1, \mathcal{O}_2](r)}{G_T[1, 1](r)} \right\rangle \quad (30)$$

and

$$\mathcal{G}[\mathcal{O}_1, \mathcal{O}_2, r]' := \frac{\langle G_T^c[\mathcal{O}_1, \mathcal{O}_2](r) \rangle}{\langle G_T[1, 1](r) \rangle} \quad (31)$$

respectively. If we take the correlator (28) as our starting point, we obtain

$$\mathcal{G}_q[\mathcal{O}_1, \mathcal{O}_2, r] := \langle \tilde{G}_{T,q}^c[\mathcal{O}_1, \mathcal{O}_2](r) \rangle = \left\langle \frac{G_{T,q}^c[\mathcal{O}_1, \mathcal{O}_2](r)}{G_T[1, 1](r)} \right\rangle \quad (32)$$

and

$$\mathcal{G}_q[\mathcal{O}_1, \mathcal{O}_2, r]' := \frac{\langle G_{T,q}^c[\mathcal{O}_1, \mathcal{O}_2](r) \rangle}{\langle G_T[1, 1](r) \rangle} \quad (33)$$

as possible choices. Our general expectation is that they will not differ much in the parameter region where the measurements are not subject to significant short-distance discretization artefacts or finite-size effects. We have already commented

briefly on the two different mean subtractions underlying the difference between (30) and (32) and between (31) and (33), corresponding to subtracting the manifold mean $\overline{\mathcal{O}}_i|_T$ and its ensemble average $\langle \overline{\mathcal{O}}_i|_T \rangle$ respectively when defining the connected correlator. However, for any (quasi-)local quantity \mathcal{O} , we expect the amount of self-averaging (on the same geometry) to increase as the geometries T grow in volume, such that the manifold averages approach the ensemble average ever more closely. Of course, such assumptions need to be checked in explicit situations, especially when long-range correlations may be present. Even if certain quantities can be shown to become independent in an infinite-volume limit, we are working with finite volumes where different prescriptions may differ appreciably. From a practical point of view, some choices of correlators may be less sensitive to finite-size effects than others, and therefore preferable. We have run explicit tests of the two different subtraction prescriptions for the normalized correlators of the local vertex degree or coordination number $c(x)$ (the number of triangles meeting at the vertex x) and the average sphere distance \bar{d} and did not observe any differences within measuring accuracy.

The situation regarding the difference between the two normalizations, i.e. between (30) and (31) and between (32) and (33), is similar. Recalling that $G_T[1, 1](r) = N_0(T)\text{vol}(S^r)|_T$, we see that this difference depends on the variance

$$\sigma_{\text{vol}(S^r)|_T}^2 = \langle \overline{\text{vol}(S^r)}|_T^2 \rangle - \langle \overline{\text{vol}(S^r)}|_T \rangle^2. \quad (34)$$

For $\sigma_{\text{vol}(S^r)|_T}^2 = 0$, the two normalizations would be identical. We have verified that the variance (34) decreases as a function of volume, for all distances r . Fig. 5 shows the square root of the variance relative to the ensemble mean $\langle \overline{\text{vol}(S^r)}|_T \rangle$ of the sphere volume. Within error bars, this quantity decreases monotonically for all radii r , from the smallest volume $N_2 = 50\text{k}$ (top curve) to the largest one $N_2 = 300\text{k}$ (bottom curve). For the largest volume, the relative deviation lies below or around half a percent in the trusted r -range, which is indeed small. In addition, we have verified explicitly that the measured normalized connected correlators for the coordination number and the sphere distance for both normalization prescriptions overlap within statistical error bars.

To summarize, for the measurement of curvature correlators in 2D CDT, all variants (30)–(33) presented above seem to give equivalent results. In our quantitative analysis below, we have made the specific choices to normalize the correlators by $G_T[1, 1](r)$ *before* taking the ensemble average, and to always use a subtraction by the ensemble average to obtain connected correlators, which corresponds to option (32).

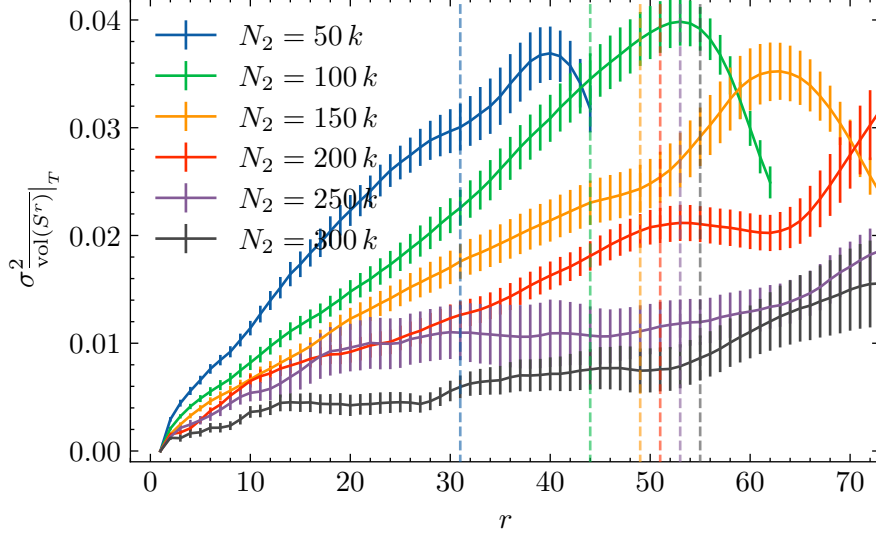


Figure 5: Relative deviation of the manifold average of the sphere volume $\text{vol}(S^r)$ from its ensemble average, as a function of the sphere radius r , for volumes $N_2 \in [50k, 300k]$. Vertical dashed lines indicate the upper end r_{max} of the trusted r -range (cf. Appendix A). The relatively large error bars come from using only about 100 configurations.

5.3 Measuring curvature correlators

With all necessary ingredients in place, we can now investigate the normalized, diffeomorphism-invariant connected two-point curvature correlators of 2D CDT. In accordance with our discussion of the quantum Ricci curvature or, more precisely, the quantum Ricci scalar in Sec. 4, the (quasi-)local scalar quantity associated with a vertex x whose correlator we will consider is the normalized average sphere distance $\bar{d}(S_x^\delta, S_x^\delta)/\delta$ of eq. (11), for which we will also use the shorthand $\bar{d}_x(\delta)/\delta$ or just \bar{d}_x/δ for notational simplicity.

We have already seen that the expectation value of the manifold average of this quantity has a specific, nontrivial δ -dependence (Fig. 4). To determine the corresponding two-point correlation functions involves measuring \bar{d}/δ at a given sphere radius δ for point pairs (x, y) , which are a geodesic link distance r apart, as illustrated schematically by Fig. 6. In the present study, we will average over all point pairs, and not distinguish between space- and time-like separations between points, to the extent these concepts can be said to be “inherited” from the Lorentzian geometries before the Wick rotation, which is not completely straightforward.

Recall that the computation of the average distance $\bar{d}(\delta)$ of a sphere S^δ to itself depends on the patch of geometry contained inside the sphere. We therefore

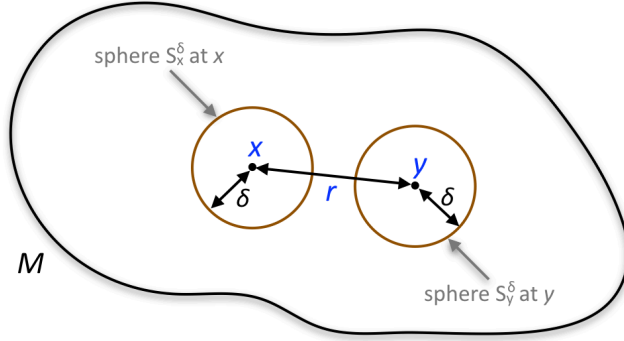


Figure 6: Schematic illustration of the contribution of an individual point pair (x, y) at geodesic distance r to the two-point curvature correlator on the space M . Measurements of the normalized average sphere distances \bar{d}_x/δ and \bar{d}_y/δ for spheres S_x^δ and S_y^δ of the same radius δ will be correlated, for $\delta \in [8, 18]$.

expect to find correlations between the quasi-local quantities $\bar{d}_x(\delta)$ and $\bar{d}_y(\delta)$ whenever the two spheres intersect or touch, i.e. whenever $r \leq 2\delta$, and possibly slightly beyond. Of course, these correlations are spurious in the sense that they are there by construction, due to the fact that we need a whole vertex neighbourhood to determine the local curvature. They will not be considered for the continuum analysis.

All simulations described in this section were performed at fixed two-volumes $N_2 = 100k, 200k$ and $300k$, and sphere sizes of even radius δ in the interval $\delta \in [8, 18]$. This range corresponds to the initial rise of the curvature profile beyond the region of lattice artefacts for small δ . For each volume used, we have determined a maximal distance r_{\max} , below which finite-size effects are considered negligible, as explained further in Appendix A. The data points relevant for a physical continuum interpretation therefore lie in the region $2\delta < r \lesssim r_{\max}$.

The ensemble average was estimated by using 150 configurations sampled via the Markov chain Monte Carlo algorithm, where we performed $N_2 \times 200$ Monte Carlo moves between subsequent measurements. The statistical errors have been estimated using a batched bootstrapping method to account for possible correlations between successive samples of configurations in the Monte Carlo algorithm. Since our moves are rejection-free, this means that each site of the geometry was on average updated 200 times. In each of the 150 triangulations, the correlator (35) was estimated by sampling 5000 vertex pairs uniformly. To the best of our knowledge, our methodology for implementing a uniform sampling is new, and different from related prescriptions in the literature, which seem to contain a systematic bias. This is explained in more detail in Appendix B.

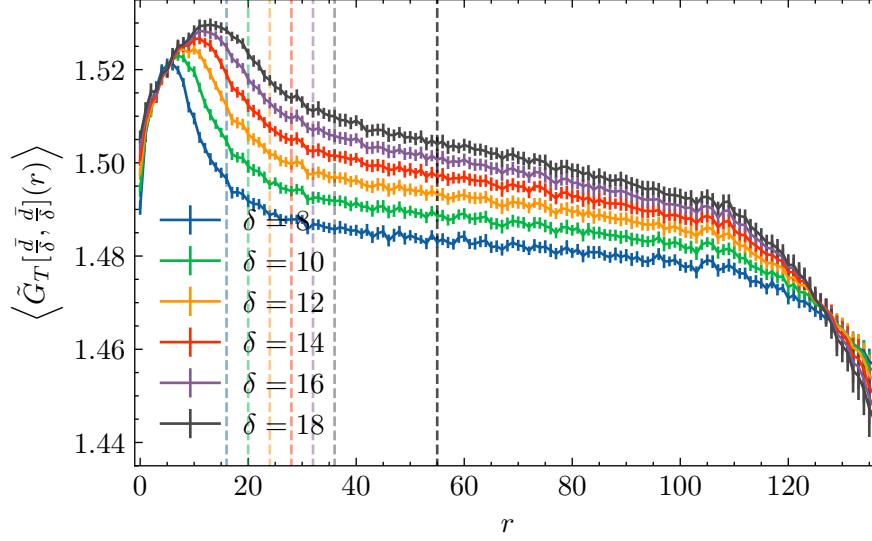


Figure 7: Normalized curvature correlator $\langle \tilde{G}_T[\frac{\bar{d}}{\delta}, \frac{\bar{d}}{\delta}](r) \rangle$ as a function of the link distance r , for volume $N_2=300k$ and various sphere radii $\delta \in [8, 18]$. The vertical dashed line of matching colour indicates the value $r=2\delta$ below which we expect correlations to be spurious. The black vertical dashed line marks the radius $r_{\max}=55$ below which finite-size effects are negligible.

We start by reporting the results of the normalized curvature correlator

$$\langle \tilde{G}_T[\frac{\bar{d}}{\delta}, \frac{\bar{d}}{\delta}](r) \rangle = \left\langle \frac{G_T[\frac{\bar{d}}{\delta}, \frac{\bar{d}}{\delta}](r)}{G_T[1, 1](r)} \right\rangle. \quad (35)$$

The plot of the measurement data for the largest volume $N_2=300k$ is shown in Fig. 7. We observe that for each δ , the measured correlator (35) starts out with a peak that lies almost entirely inside $r \leq 2\delta$, then decreases gently as a function of r throughout the trusted r -range, before taking a steeper drop around $r \approx 110$, far beyond r_{\max} . Unsurprisingly, the width and height of the initial peak grows for larger values of δ , indicating stronger correlations due to the larger size of the overlap region between the interiors of the two spheres.

Next, let us look at the measurements of the normalized correlator of the curvature with the unit operator,

$$\langle \tilde{G}_T[\frac{\bar{d}}{\delta}, 1](r) \rangle = \left\langle \frac{G_T[\frac{\bar{d}}{\delta}, 1](r)}{G_T[1, 1](r)} \right\rangle = \left\langle \frac{\sum_{x,y \in T} \frac{\bar{d}_x}{\delta} \delta_{d(x,y),r}}{\sum_{x,y \in T} \delta_{d(x,y),r}} \right\rangle, \quad (36)$$

shown in Fig. 8. As anticipated in Secs. 5.1 and 5.2, due to the non-constancy of the geometry there are nontrivial correlations between the average sphere distance \bar{d}_x and the Kronecker delta $\delta_{d(x,y),r}$ in $G_T[\frac{\bar{d}}{\delta}, 1](r)$, such that (36) is not equal to the

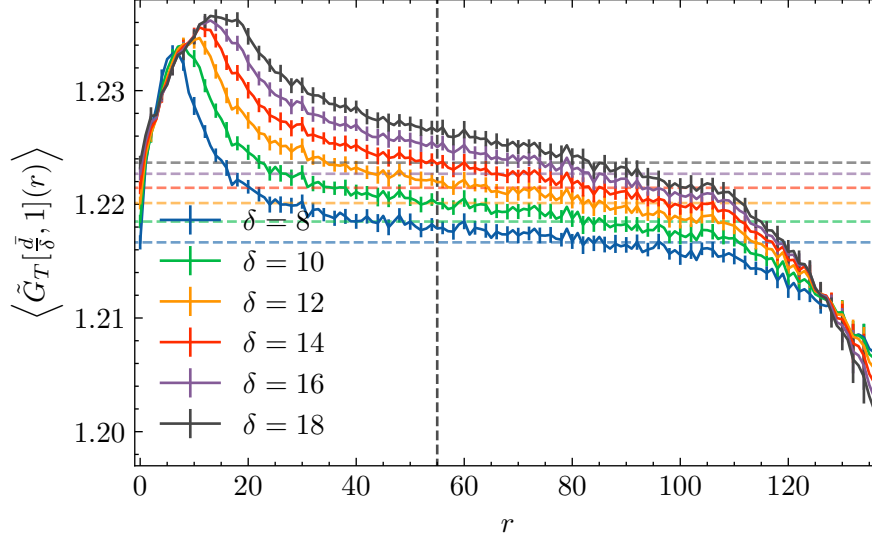


Figure 8: Normalized correlator $\langle \tilde{G}_T[\frac{\bar{d}}{\delta}, 1](r) \rangle$ as a function of the link distance r , together with the ensemble average $\langle \bar{d}/\delta|_T \rangle$ (dashed horizontal line of matching colour), for volume $N_2 = 300k$ and various sphere radii $\delta \in [8, 18]$.

ensemble average $\langle \bar{d}/\delta|_T \rangle$, which we have included in the figure for comparison. Note that the shapes of the curves for $\langle \tilde{G}_T[\frac{\bar{d}}{\delta}, 1](r) \rangle$ in Fig. 8 are rather similar to those for $\langle \tilde{G}_T[\frac{\bar{d}}{\delta}, \frac{\bar{d}}{\delta}](r) \rangle$ in Fig. 7. We will analyze next how they combine when we determine the connected correlator.

Fig. 9 shows the Monte Carlo measurements for the connected curvature correlator

$$\mathcal{G}_q[\frac{\bar{d}}{\delta}, \frac{\bar{d}}{\delta}, r] = \langle \tilde{G}_T[\frac{\bar{d}}{\delta}, \frac{\bar{d}}{\delta}](r) \rangle - 2\langle \bar{d}/\delta|_T \rangle \langle \tilde{G}_T[\frac{\bar{d}}{\delta}, 1](r) \rangle + \langle \bar{d}/\delta|_T \rangle^2, \quad (37)$$

whose general form was defined in eq. (32). The most striking feature of this correlator is that it vanishes identically within measuring accuracy outside $r \leq 2\delta$, independent of the value of δ for which we measure the average sphere distance. In other words, we find a perfect cancellation among the nonvanishing terms on the right-hand side of eq. (37), which even extends to distances r significantly above the trusted range $2\delta < r \lesssim 55$. The deviations from zero that appear for $r \gtrsim 120$ are due to finite-size effects.¹⁵ For small r , $0 \leq r \lesssim 2\delta$, we observe a qualitatively similar behaviour for all values of δ , namely an initially positive correlation, which for growing r dips briefly into negative territory before going to zero at $r \approx 2\delta$. We do not have an explanation for the detailed behaviour of these curves; correlations are clearly present, caused by the overlap of the interiors

¹⁵We have also measured the connected correlators for smaller volumes N_2 , where the results are similar, but the finite-size effects set in at smaller values of r .

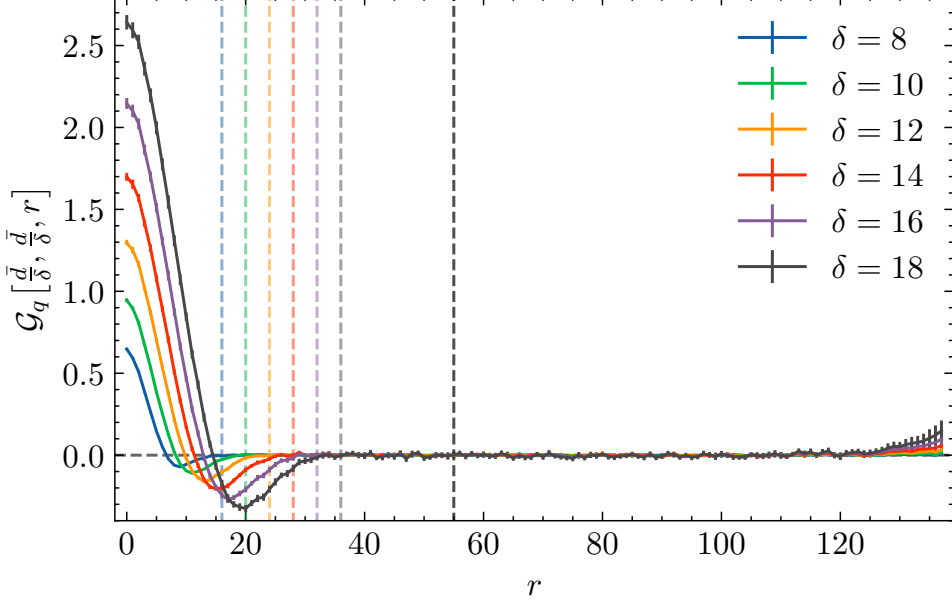


Figure 9: Normalized connected curvature correlator $\mathcal{G}_q[\frac{\bar{d}}{\delta}, \frac{\bar{d}}{\delta}, r]$ as a function of the link distance r for volume $N_2=300k$ and various sphere radii $\delta \in [8, 18]$.

of the spheres, but these are mixed with short-distance discretization artefacts, which are known to affect the average sphere distance for small δ . At any rate, we do not expect this region to be associated with interesting continuum physics.

Note that a “naïve” subtraction

$$\langle \tilde{G}_T[\frac{\bar{d}}{\delta}, \frac{\bar{d}}{\delta}](r) \rangle - \langle \overline{\bar{d}/\delta} |_T \rangle^2, \quad (38)$$

which would be appropriate for a connected correlator of local quantum fields on a fixed, flat background, in our case does not produce a vanishing result, because the first term has a nontrivial r -dependence (cf. Fig. 7), while the second one is constant. Since the correlator vanishes inside the relevant r -ranges for all volumes we have investigated, a finite-size scaling analysis, where one overlaps measurements after rescaling distances according to $r \rightarrow r/N_2^{1/d_H} = r/N_2^{1/2}$, is straightforward and compatible with a vanishing continuum correlator.

From a physical viewpoint the vanishing of the curvature correlator $\mathcal{G}_q[\frac{\bar{d}}{\delta}, \frac{\bar{d}}{\delta}, r]$ has a clear-cut interpretation: because of the absence of local propagating degrees of freedom in two-dimensional quantum gravity, we do not expect to find correlations between *any* local geometric operators. Our measurements confirm this expectation and at the same time strengthen confidence in the construction of manifestly diffeomorphism-invariant correlators in nonperturbative quantum gravity, and the feasibility of computing correlators of the quantum Ricci curvature in particular.

6 Summary and outlook

We have presented above the first quantitative analysis of diffeomorphism-invariant two-point correlators of the curvature in nonperturbative Lorentzian quantum gravity, albeit in a two-dimensional toy model. Another novel feature was the use in the correlator of the quantum Ricci curvature, a notion of curvature geared towards nonperturbative lattice quantum gravity, with an improved UV behaviour compared to other prescriptions [21]. We have demonstrated that the construction and numerical implementation of these correlators is conceptually and technically feasible and leads to a physically sensible result, namely the vanishing of the connected curvature correlator (37) within measuring accuracy.

Our analysis highlighted unexpected structural features of the connected correlators, which are due to the dynamical nature of the geometry and would not be present on a fixed, flat background space(-time). They lead to ambiguities in the definition of these correlators, which turned out to be immaterial in 2D Lorentzian quantum gravity, but may well be important in other cases.

With the study of correlators in nonperturbative quantum gravity still in its infancy, the successful completion of our two-dimensional implementation is very encouraging for their further development. As mentioned in the introduction, our main motivation is the investigation of curvature correlators in full, four-dimensional quantum gravity in a near-Planckian regime, using the technical framework of lattice gravity based on CDT. From a cosmological perspective, it would be very interesting to measure correlators associated with spacelike hypersurfaces in the emergent de Sitter-like quantum universe found in this formulation. In standard early-universe cosmology, such correlators describe the quantum fluctuations of a hypothetical inflaton field, which act as seeds of primordial inhomogeneities in a de Sitter-like background spacetime, and are also directly related to the so-called power spectrum [62, 63]. If we can derive correlators and their properties from first principles in nonperturbative quantum gravity, this may provide a purely quantum-gravitational explanation and possibly new predictions for the nature of these fluctuations in cosmology, without resorting to additional matter fields. This is the subject of ongoing research we hope to report on elsewhere.

Acknowledgments

RL thanks the Perimeter Institute for hospitality. This research was supported in part by Perimeter Institute for Theoretical Physics. Research at Perimeter Institute is supported by the Government of Canada through the Department of Innovation, Science and Economic Development and by the Province of Ontario through the Ministry of Colleges and Universities.

Appendix A

In this appendix, we explain the method we have used to establish a range of distances $r \lesssim r_{\max}$ where finite-size effects in the measurements of the correlators $\langle \tilde{G}(r) \rangle$, $\mathcal{G}_q[r]$ presented in Sec. 5.3 are negligible. It is related to what we call the *effective linear size* L of a typical triangulation in an ensemble at fixed two-volume. This is an approximate concept, which we obtain by monitoring the discrete volume of a 2D ball B_x^r (all triangles contained inside the sphere S_x^r), as one would do when extracting the Hausdorff dimension d_H from the leading scaling behaviour of the expectation value $\langle \text{vol}(B^r) \rangle \propto r^{d_H}$. As we increase the ball radius r on triangulations of a given volume N_2 , this scaling will start deviating from a power law once the typical ball wraps around the spatial direction of the torus and starts to selfoverlap.¹⁶ We then identify the length L as the diameter $2r_{\max}$ of the largest typical ball whose selfoverlaps are sufficiently small not to affect the (quadratic) power-law scaling of its volume significantly. The linear size L is therefore also a rough estimate of the length of a typical shortest, noncontractible geodesic that wraps once around the spatial direction of the torus. We have made rather conservative choices, such that r_{\max} is located well below the radius where a deviation from a single power law becomes visible in the volume plots (see [53] for technical details). Half of the linear scale L then gives us a maximal distance $r_{\max} = L/2$ below which we are confident that the influence of finite-size effects on the correlators is negligible. For the volumes $N_2 = \{50\text{k}, 100\text{k}, 150\text{k}, 200\text{k}, 250\text{k}, 300\text{k}\}$, the maximal distances obtained in this way are $r_{\max} = \{31, 44, 49, 51, 53, 55\}$ respectively.

Appendix B

An important element of the computational implementation of the two-point correlators described in the main text is a uniform sampling of point pairs (x, y) at a given discrete distance r . It is feasible to evaluate the average over all point pairs (x, y) fully, but it is significantly more effective computationally to estimate this average with a sample of point pairs. Uniformity of this sampling is defined with respect to the volume weight, which is 1 for each vertex. Accordingly, all pairs of vertices (x, y) , $d(x, y) = r \neq 0$, should also have equal weight and be selected with the same probability. Since the underlying geometries are irregular random triangulations, such a uniform sampling is slightly nontrivial. A straightforward implementation for a given geometry T would be to create a complete list of all vertex pairs at distance r , and sample uniformly from this set. However, creating

¹⁶The time extensions t_{tot} of our triangulations are such that wrapping in the spatial direction always happens much before it would occur in the time direction, see also footnote 5.

such a list requires identifying all vertex pairs, in which case one could perform the full sum over all point pairs without additional computational cost. In this case, one would not gain any computational benefit from sampling, especially since we tend to require only relatively small samples to estimate manifold averages.

Note that the same sampling issue arises in measurements of the (average) quantum Ricci curvature, whenever one uses the prescription involving the average sphere distance of two δ -spheres whose centres are a distance δ apart, obtained by setting $\varepsilon = \delta$ in the defining relation (8). In this situation, one also needs to sample vertex pairs (p, p') at a prescribed distance. This was implemented in previous work [10, 14, 46] by (i) uniformly sampling a first vertex $p \in T$, (ii) constructing the δ -sphere S_p^δ around p , and (iii) selecting a second vertex p' uniformly from S_p^δ . This is a much more efficient method, since it only requires a single breadth-first search for every vertex pair (as opposed to $N_0(T)$ breadth-first searches for all vertex pairs), but it does not amount to a uniform sampling of point pairs! Instead, the second vertex p' is chosen with a relative weight $1/\text{vol}(S_p^\delta)$, which depends on p . These weights would all be identical if the geometry was completely regular and the neighbourhood of each vertex looked the same, but this is of course generally not the case.

To what extent the bias resulting from this nonuniform sampling is significant, in the sense of affecting continuum outcomes, is not immediately clear. In general, its effect will depend both on the observable studied and the nature of the typical geometry in the ensemble. Previous studies of correlators in EDT [34, 61] do not specify their methodology explicitly, but may also have used a nonuniform sampling. With growing vertex distance, the bias can decrease if the individual sphere volumes become more similar to their manifold average. We have found some evidence for the latter in the 2D CDT data, but it is not sufficiently stringent to draw any general conclusion about the equivalence or otherwise of the two sampling methods. We have not attempted a comprehensive analysis of their difference either, but have repeated the measurement of the curvature profile $\langle \bar{d}_{\text{av}}(\delta)/\delta \rangle$ for $\varepsilon = \delta$ in 2D CDT of reference [46] with a uniform sampling. The main net effect outside the region of lattice artefacts is a small vertical upward shift of the data points, compared to the nonuniform sampling [53]. Since the vertical offset of the curvature profile is known to be not universal, the influence of the samplings on this particular observable seems rather mild, at least in the range $N_2 \leq 300\text{k}$ of volumes considered, which is reassuring with regard to the validity of the earlier investigations of curvature profiles.

Having pinpointed the origin of the nonuniformity, we can modify the corresponding sampling in a straightforward way to make it “effectively uniform” while still taking advantage of its computational simplicity, by including compensating weight factors. The modified sampling prescription is as follows: (i)' pick a first vertex $x \in T$ uniformly at random, (ii)' construct the r -sphere S_x^r around x ,

(iii)' select a second vertex y uniformly from S_x^r , and (iv)' multiply the measurement associated with the point pair (x, y) by a weight factor $\text{vol}(S_x^r)/\overline{\text{vol}(S^r)}|_T$. There is no extra computational cost in this last step, since the sphere S_x^r has to be determined in any case. We have tested this weighted sampling method for the two-point correlator of the coordination number $c(x)$ in 2D CDT, and verified that within statistical error bars it leads to identical results for the same quantity sampled uniformly by using complete lists of point pairs, as described earlier. All correlator measurements in this paper have been performed by using the weighted, effectively uniform sampling.

References

- [1] J. Ambjørn, A. Görlich, J. Jurkiewicz and R. Loll, *Nonperturbative quantum gravity*, Phys. Rep. 519 (2012) 127-210 [arXiv:1203.3591, hep-th].
- [2] R. Loll, *Quantum gravity from causal dynamical triangulations: A review*, Class. Quant. Grav. 37 (2020) 013002 [arXiv:1905.08669, hep-th].
- [3] J. Ambjørn and R. Loll, *Causal dynamical triangulations: Gateway to non-perturbative quantum gravity*, to appear in *Encyclopedia of Mathematical Physics 2nd Edition*, eds. M. Bojowald and R.J. Szabo [arXiv:2401.09399, hep-th].
- [4] J. Ambjørn, J. Jurkiewicz and R. Loll, *Emergence of a 4-D world from causal quantum gravity*, Phys. Rev. Lett. 93 (2004) 131301 [arXiv:hep-th/0404156].
- [5] J. Ambjørn, J. Jurkiewicz and R. Loll, *The spectral dimension of the universe is scale-dependent*, Phys. Rev. Lett. 95 (2005) 171301 [arXiv:hep-th/0505113].
- [6] J. Ambjørn, J. Jurkiewicz and R. Loll, *Reconstructing the universe*, Phys. Rev. D 72 (2005) 064014, [arXiv:hep-th/0505154].
- [7] J. Ambjørn, A. Görlich, J. Jurkiewicz and R. Loll, *Planckian birth of the quantum de Sitter universe*, Phys. Rev. Lett. 100 (2008) 091304 [arXiv:0712.2485, hep-th].
- [8] J. Ambjørn, A. Görlich, J. Jurkiewicz and R. Loll, *The nonperturbative quantum de Sitter universe*, Phys. Rev. D 78 (2008) 063544 [arXiv:0807.4481, hep-th].
- [9] J. Ambjørn, A. Görlich, J. Jurkiewicz, R. Loll, J. Gizbert-Studnicki and T. Trzesniewski, *The semiclassical limit of Causal Dynamical Triangulations*, Nucl. Phys. B 849 (2011) 144-165 [arXiv:1102.3929, hep-th].

- [10] N. Klitgaard and R. Loll, *How round is the quantum de Sitter universe?*, Eur. Phys. J. C 80 (2020) 990 [arXiv:2006.06263, hep-th].
- [11] W. Donnelly and S.B. Giddings, *Observables, gravitational dressing, and obstructions to locality and subsystems*, Phys. Rev. D 94 (2016) 104038 [arXiv:1607.01025, hep-th].
- [12] M. Fröb and W. Lima, *Propagators for gauge-invariant observables in cosmology*, Class. Quant. Grav. 35 (2018) 095010 [arXiv:1711.08470, gr-qc].
- [13] N. Klitgaard and R. Loll, *Introducing quantum Ricci curvature*, Phys. Rev. D 97 (2018) 046008 [arXiv:1712.08847, hep-th].
- [14] N. Klitgaard and R. Loll, *Implementing quantum Ricci curvature*, Phys. Rev. D 97 (2018) 106017 [arXiv:1802.10524, hep-th].
- [15] J. Ambjørn, J. Jurkiewicz and R. Loll, *The spectral dimension of the universe is scale-dependent*, Phys. Rev. Lett. 95 (2005) 171301 [arXiv:hep-th/0505113].
- [16] S. Carlip, *Dimension and dimensional reduction in quantum gravity*, Class. Quant. Grav. 34 (2017) 193001 [arXiv:1705.05417, gr-qc],
- [17] D. Oriti, ed., *Approaches to quantum gravity*, Cambridge University Press (2009), doi: 10.1017/CBO9780511575549.
- [18] J. Murugan, A. Weltman and G.F.R. Ellis, eds., *Foundations of space and time: reflections on quantum gravity*, Cambridge University Press (2012), doi: 10.1017/CBO9780511920998.
- [19] J. Armas, ed., *Conversations on quantum gravity*, Cambridge University Press (2021), doi: 10.1017/9781316717639.
- [20] R. Loll, G. Fabiano, D. Frattulillo and F. Wagner, *Quantum gravity in 30 questions*, PoS (CORFU2021) 316 [arXiv:2206.06762, hep-th].
- [21] R. Loll, *Quantum curvature as key to the quantum universe*, in *Handbook of Quantum Gravity*, eds. C. Bambi, L. Modesto and I.L. Shapiro, Springer, Singapore (2024) [arXiv:2306.13782, gr-qc].
- [22] I. Montvay and G. Münster, *Quantum fields on a lattice*, Cambridge University Press (1997), doi: 10.1017/CBO9780511470783.
- [23] I.L. Shapiro, *The background information about perturbative quantum gravity* [arXiv:2210.12319, hep-th].

- [24] N. Christiansen, B. Knorr, J. Meibohm, J.M. Pawłowski and M. Reichert, *Local quantum gravity*, Phys. Rev. D 92 (2015) 121501 [arXiv:1506.07016, hep-th].
- [25] L. Parker and D. Toms, *Quantum field theory in curved spacetime*, Cambridge University Press (2009), doi: 10.1017/CBO9780511813924.
- [26] J. Ambjørn, J. Jurkiewicz, and C. Kristjansen, *Quantum gravity, dynamical triangulations and higher derivative regularization*, Nucl. Phys. B 393 (1993) 601–632 [arXiv:hep-th/9208032].
- [27] J. Ambjørn and J. Jurkiewicz, *Scaling in four-dimensional quantum gravity*, Nucl. Phys. B 451 (1995) 643–676 [arXiv:hep-th/9503006].
- [28] J. Ambjørn and Y. Watabiki, *Scaling in quantum gravity*, Nucl. Phys. B 445 (1995) 129–144 [arXiv:hep-th/9501049, hep-th].
- [29] J. Ambjørn, J. Jurkiewicz and Y. Watabiki, *On the fractal structure of two-dimensional quantum gravity*, Nucl. Phys. B 454 (1995) 313–342 [arXiv:hep-lat/9507014].
- [30] H. Aoki, H. Kawai, J. Nishimura and A. Tsuchiya, *Operator product expansion in two-dimensional quantum gravity*, Nucl. Phys. B 474 (1996) 512–528 [arXiv:hep-th/9511117].
- [31] J. Ambjørn and K. Anagnostopoulos, *Quantum geometry of 2-D gravity coupled to unitary matter*, Nucl. Phys. B 497 (1997) 445–478 [arXiv:hep-lat/9701006].
- [32] J. Ambjørn, C. Kristjansen and Y. Watabiki, *The two point function of $c = -2$ matter coupled to 2-D quantum gravity*, Nucl. Phys. B 504 (1997) 555–579 [arXiv:hep-th/9705202].
- [33] J. Ambjørn, P. Bialas and J. Jurkiewicz, *Connected correlators in quantum gravity*, JHEP 02 (1999) 005 [arXiv:hep-lat/9812015].
- [34] B. de Bakker and J. Smit, *Two point functions in 4-D dynamical triangulation*, Nucl. Phys. B 454 (1995) 343–356 [arXiv:hep-lat/9503004].
- [35] P. Bialas, Z. Burda, A. Krzywicki and B. Petersson, *Focusing on the fixed point of 4-D simplicial gravity*, Nucl. Phys. B 472 (1996) 293–308 [arXiv:hep-lat/9601024].
- [36] S.D. Bassler, *Euclidean dynamical triangulations: Running couplings and curvature correlation functions*, PhD thesis Syracuse University (2019), link: surface.syr.edu/etd/1104.

- [37] T. Regge, *General relativity without coordinates*, Nuovo Cim. 19 (1961) 558–571, doi: 10.1007/BF02733251.
- [38] J. Ambjørn and J. Jurkiewicz, *Four-dimensional simplicial quantum gravity*, Phys. Lett. B 278 (1992) 42–50, doi: 10.1016/0370-2693(92)90709-D.
- [39] J. Ambjørn, S. Jordan, J. Jurkiewicz and R. Loll, *A second-order phase transition in CDT*, Phys. Rev. Lett. 107 (2011) 211303 [arXiv:1108.3932, hep-th].
- [40] J. Ambjørn, S. Jordan, J. Jurkiewicz and R. Loll, *Second- and first-order phase transitions in CDT*, Phys. Rev. D 85 (2012) 124044 [arXiv:1205.1229, hep-th].
- [41] D. Coumbe, J. Gizbert-Studnicki and J. Jurkiewicz, *Exploring the new phase transition of CDT*, JHEP 1602 (2016) 144 [arXiv:1510.08672, hep-th].
- [42] J. Ambjørn and R. Loll, *Nonperturbative Lorentzian quantum gravity, causality and topology change*, Nucl. Phys. B 536 (1998) 407-434 [arXiv:hep-th/9805108].
- [43] J. Ambjørn, J. Jurkiewicz and R. Loll, *Dynamically triangulating Lorentzian quantum gravity*, Nucl. Phys. B 610 (2001) 347-382 [arXiv:hep-th/0105267].
- [44] B. Durhuus, T. Jonsson and J.F. Wheeler, *On the spectral dimension of causal triangulations*, J. Statist. Phys. 139 (2010) 859-881 [arXiv:0908.3643, math-ph].
- [45] P. Di Francesco, E. Guitter and C. Kristjansen, *Integrable 2-D Lorentzian gravity and random walks*, Nucl. Phys. B 567 (2000) 515-553 [arXiv:hep-th/9907084].
- [46] J. Brunekreef and R. Loll, *Quantum flatness in two-dimensional quantum gravity*, Phys. Rev. D 104 (2021) 126024 [arXiv:2110.11100, hep-th].
- [47] J. Brunekreef and R. Loll, *Curvature profiles for quantum gravity*, Phys. Rev. D 103 (2021) 026019 [arXiv:2011.10168, gr-qc].
- [48] M.E.J. Newman and G.T. Barkema, *Monte Carlo methods in statistical physics*, Oxford University Press (1999), doi: 10.1093/oso/9780198517962.001.0001.
- [49] J. Ambjørn, B. Durhuus and T. Jonsson, *Quantum geometry: A statistical field theory approach*, Cambridge University Press (1997), doi: 10.1017/CBO9780511524417.

- [50] see <https://www.rust-lang.org/>
- [51] J. van der Duin, Source code for simulating 2D causal dynamical triangulations in Rust, link: gitlab.com/dynamical-triangulation/dyntri.
- [52] J. Ambjørn, K.N. Anagnostopoulos and R. Loll, *A new perspective on matter coupling in 2d quantum gravity*, Phys. Rev. D 60 (1999) 104035, doi: 10.1103/PhysRevD.60.104035 [arXiv:hep-th/9904012].
- [53] J. van der Duin, *Curvature correlations in quantum gravity*, Master Thesis, Radboud University (2023), link: www.ru.nl/highenergyphysics/theses/master-theses.
- [54] J. Brunekreef, A. Görlich and R. Loll, *Simulating CDT quantum gravity*, Comput. Phys. Commun. 300 (2024) 109170 [arXiv:2310.16744, hep-th].
- [55] Y. Ollivier, *A visual introduction to Riemannian curvatures and some discrete generalizations*, in Analysis and Geometry of Metric Measure Spaces, eds. G. Dafni, R. McCann and A. Stancu, CRM Proceedings and Lecture Notes 56 (2013), American Mathematical Society, doi: 10.1090/crmp/056.
- [56] Y. Ollivier, *Ricci curvature of Markov chains on metric spaces*, J. Funct. Anal. 256 (2009) 810-864, doi: 10.1016/j.jfa.2008.11.001.
- [57] L. Brewin, *Riemann normal coordinate expansions using Cadabra*, third version, Nov 2022, see also Class. Quant. Grav. 26 (2009) 175017 [arXiv:0903.2087v3, gr-qc].
- [58] J. van der Duin and A. Silva, *Scalar curvature for metric spaces: Defining curvature for quantum gravity without coordinates* [arXiv:2311.07507, hep-th].
- [59] G. Modanese, *Vacuum correlations at geodesic distance in quantum gravity*, Riv. Nuovo Cim. 17N8 (1994) 1–62 [arXiv:hep-th/9410086].
- [60] M.B. Fröb, *One-loop quantum gravitational corrections to the scalar two-point function at fixed geodesic distance*, Class. Quant. Grav. 35 (2018) 035005 [arXiv:1706.01891, hep-th].
- [61] P. Bialas, *Correlations in fluctuating geometries*, Nucl. Phys. B Proc. Suppl. 53 (1997) 739–742 [arXiv:hep-lat/9608029].
- [62] V. Mukhanov, *Physical Foundations of Cosmology*, Cambridge University Press (2005), doi: 10.1017/CBO9780511790553.

- [63] G.F.R. Ellis, R. Maartens and M.A.H. MacCallum, *Relativistic Cosmology*, Cambridge University Press (2012), doi: 10.1017/CBO9781139014403.